THE JOURNAL OF PHYSICAL CHEMISTRY B

Article

pubs.acs.org/JPCB

# Exploration of the Singlet $O_2$ Oxidation of 8-Oxoguanine by Guided-Ion Beam Scattering and Density Functional Theory: Changes of Reaction Intermediates, Energetics, and Kinetics upon Protonation/Deprotonation and Hydration

Yan Sun,[†,‡] Wenchao Lu,[†,‡] and Jianbo Liu*[,†,‡]

[†]Department of Chemistry and Biochemistry, Queens College of the City University of New York, 65-30 Kissena Blvd., Queens, New York 11367, United States

[‡]Ph.D. Program in Chemistry, The Graduate Center of the City University of New York, 365 Fifth Ave., New York, New York 10016, United States

Supporting Information

**ABSTRACT:** 8-Oxo-7,8-dihydro-2′-deoxyguanosine (8-oxodGuo) is one of the most common DNA lesions resulting from reactive oxygen species and ionizing radiation, and is involved in mutagenesis, carcinogenesis, and cell death. Notably, 8-oxodGuo is more reactive toward singlet ($a^1\Delta_g$) $O_2$ than the undamaged guanosine, and the lesions arising from the secondary oxidation of 8-oxodGuo are more mutagenic. Herein the $^1O_2$ oxidation of free base 8-oxoguanine (8-oxoG) was investigated at different initial conditions including protonated $[8\text{-oxoG} + H]^+$, deprotonated $[8\text{-oxoG} - H]^-$, and their monohydrates. Experiment was carried out on a guided-ion beam scattering tandem mass spectrometer. Measurements include the effects of collision energy ($E_{col}$) on reaction cross sections over a center-of-mass $E_{col}$ range from 0.1 to 0.5 eV. The aim of this study is to quantitatively probe the sensitivity of the early stage of 8-oxoG oxidation to ionization and hydration. Density functional theory and Rice−Ramsperger−Kassel−Marcus calculations were performed to identify the intermediates and the products along reaction pathways and locate accessible reaction potential energy surfaces, and to rationalize reaction outcomes from energetic and kinetic points of view. No product was observed for the reaction of $[8\text{-oxoG} + H]^+\cdot W_{0,1}$ ($W = H_2O$) because insurmountable barriers block the addition of $^1O_2$ to reactant ions. Neither was $[8\text{-oxoG} - H]^-$ reactive with $^1O_2$, in this case due to the rapid decay of transient intermediates to starting reactants. However, the nonreactivity of $[8\text{-oxoG} - H]^-$ was inverted by hydration; as a result, 4,5-dioxetane of $[8\text{-oxoG} - H]^-$ was captured as the main oxidation product. Reaction cross section for $[8\text{-oxoG} - H]^-\cdot W + {}^1O_2$ decreases with increasing $E_{col}$ and becomes negligible above 0.3 eV, indicating that the reaction is exothermic and has no barriers above reactants. The contrasting oxidation behaviors of $[8\text{-oxoG} + H]^+\cdot W_{0,1}$ and $[8\text{-oxoG} - H]^-\cdot W_{0,1}$, which are relevant to the pH dependence of 8-oxoG oxidation in solution, are interpreted in terms of different $^1O_2$ addition pathways.

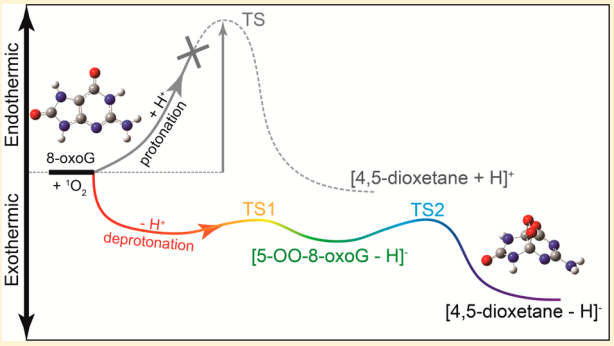


## 1. INTRODUCTION

Guanine is the most easily oxidized of the four DNA bases, and is the exclusive DNA target for singlet ($a^1\Delta_g$) $O_2$.[1−11] Depending on chemical contexts and reaction conditions, the $^1O_2$ oxidation of 2′-deoxyguanosine (dGuo) leads to formation of different products, of which 8-oxo-7,8-dihydro-2′-deoxyguanosine (8-oxodGuo) is predominant for isolated and cellular DNA.[5] 8-oxodGuo is involved in a variety of biological sequelae including mutagenesis, carcinogenesis and cell death. By mispairing with adenine during replication, 8-oxodGuo gives rise to G·C→T·A transversion—a somatic mutation in cancers.[12] 8-oxodGuo is also related to neurological disorders responsible for Alzheimer's[13] and Parkinson's diseases,[14] and triggers DNA−protein cross-linking.[15] For these reasons, 8-oxodGuo is widely used as a biomarker of "oxidative stress" within cells and tissues.[16,17]

Notably 8-oxodGuo is even more reactive toward $^1O_2$ than the undamaged dGuo,[4,5,18−25] and the lesions arising from the secondary oxidation of 8-oxodGuo are more mutagenic *in vivo* than 8-oxodGuo.[26] As summarized in Scheme 1,[19,21,23,25,27] the oxidation of 8-oxodGuo is initiated by a [2+2] addition of $^1O_2$ across the 4,5-ethylenic bond, giving rise to a transient 4,5-dioxetane (**2**). **2** was observed only in the photooxidation of 2′,3′,5′-tris(O-*tert*-butyldimethylsily)-8-oxo-7,8-dihydroguanosine in acetone or $CH_2Cl_2$.[18] The intermediate was captured by

**Received:** November 14, 2016
**Revised:** December 23, 2016
**Published:** January 6, 2017

ACS Publications © 2017 American Chemical Society



DOI: 10.1021/acs.jpcb.6b11464
J. Phys. Chem. B 2017, 121, 956−966

**Scheme 1. $^1O_2$-Induced Oxidation of 8-oxodGuo**[a]

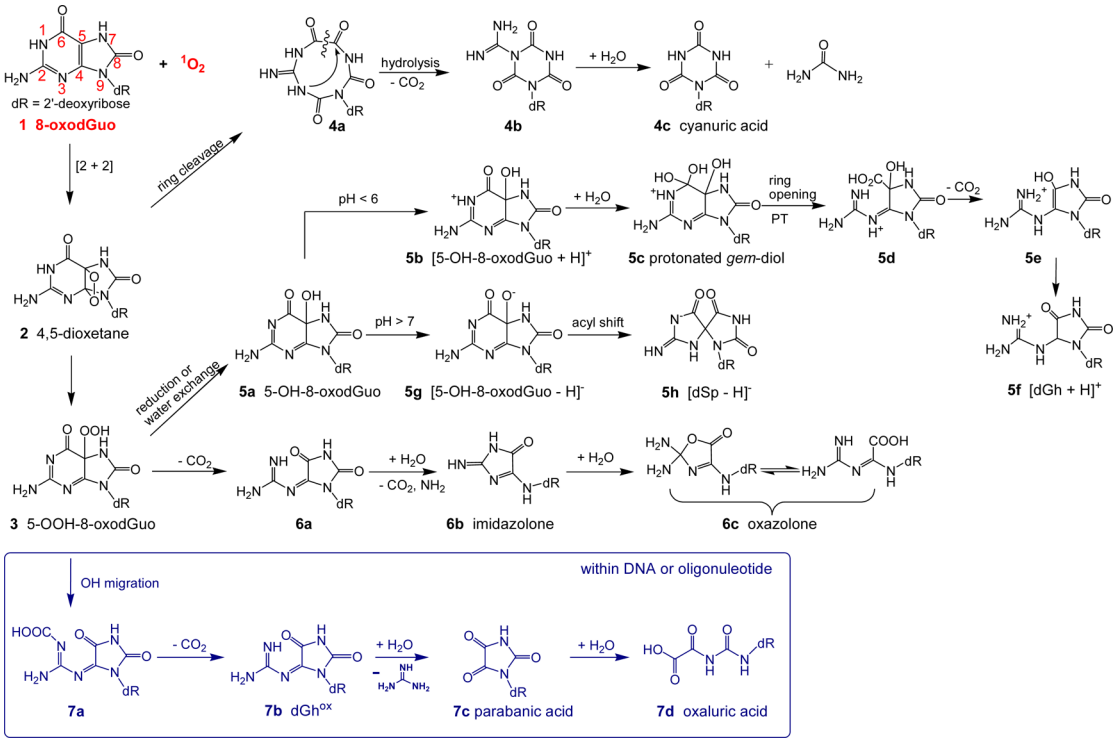


[a]Adapted from refs 19,21,23,25,27.

NMR at −80 °C, but decomposed upon warming to −60 °C. One decomposition pathway of **2** leads to 4,5-bond cleavage, producing a 9-membered macrocycle **4a**. The latter, upon intramolecular ring closure with extrusion of $CO_2$, rearranges to **4b**, and finally to cyanuric acid **4c** with concomitant release of urea.[27] Another pathway of **2** involves proton transfer and ring opening, leading to formation of a hydroperoxide 5-OOH-8-oxodGuo (**3**). **3** may either undergo reduction[23] or water exchange[3] to an alcohol 5-OH-8-oxodGuo (**5a**), or evolve into an imidazolone (**6b**) and an oxazolone (**6c**).[19] Conversion of **5a** to downstream products is pH sensitive. Under acidic conditions, formation of a protonated guanidinohydantoin ([dGh + H]$^+$, **5f**) becomes predominant, which occurs via hydrolysis of **5b**, then ring opening of **5c**, decarboxylation of **5d** and a final intramolecular H transfer of **5e**. Under neutral and basic conditions, formation of a deprotonated spiroiminodihydantoin ([dSp − H]$^-$, **5h**) is kinetically favored via an acyl migration in **5g**.[25]

The oxidation of the 8-oxodGuo residue that has been site specifically inserted into DNA or oligonucleotide follows a completely different route and appears more specific.[21] In the latter case, 5,6-bond cleavage, OH migration and subsequent $CO_2$ loss in **3** give rise to an oxidized guanidinohydantoin (dGh$^{ox}$, **7b**). Successive hydrolytic steps accompanied by the release of guanidine convert **7b** to an oxaluric acid (**7d**) through a parabanic acid (**7c**).

In light of the reaction diversity and the condition dependence of 8-oxodGuo oxidation, it is warranted to look into the reaction kinetics and dynamics, with a focus on the early stage that was not completely revealed from conventional solution-phase studies. As the ribose sugar in 8-oxodGuo makes the molecule quite larger, our first effort was targeted at the oxidation of free base 8-oxo-7,8-dihydroguanine (8-oxoG). We have examined the $^1O_2$ reactions with protonated [8-oxoG + H]$^+$ and deprotonated [8-oxoG − H]$^-$ in the gas phase and then the same systems hydrated with an explicit water molecule, using guided-ion beam scattering mass spectrometry. Reaction coordinates and potential energy surfaces (PESs) were established on the basis of density functional theory (DFT) and Rice−Ramsperger−Kassel−Marcus (RRKM)[28] analysis. As we will show, the oxidation of [8-oxoG + H]$^+$ begins by concerted cycloaddition of $^1O_2$, but all pathways are blocked by high activation barriers. On the contrary, synchronous addition does not occur to [8-oxoG − H]$^-$. The latter involves a low-energy, stepwise addition starting with formation of a 5-terminal peroxide, followed by evolving into a 4,5-dioxetane and a 5-hydroperoxide. Compared to the dehydrated systems, hydration not only changes the stabilities of protonated 8-oxoG conformations, but "cools down" the energized oxidation intermediates of deprotonated 8-oxoG, suppressing their otherwise complete decomposition back to reactants.

## 2. EXPERIMENTAL AND COMPUTATIONAL DETAILS

**2.1. Generation and Detection of $^1O_2$.** $^1O_2$ was generated by the reaction of $H_2O_2 + Cl_2 + 2KOH \rightarrow {}^1O_2/{}^3O_2 + 2KCl + 2H_2O$.[29,30] In the experiment, 10.5 mL of 8 M KOH was added to 20 mL of 35 wt% aqueous $H_2O_2$ in a sparger held at −18 °C. The resulting mixture was degassed. 3.42 sccm of $Cl_2$ (~99.5%, Sigma-Aldrich) was mixed with 53.5 sccm of He and bubbled through the $H_2O_2$/KOH slush. All of the $Cl_2$ reacted with $H_2O_2$ to produce a mixture of $^1O_2$, $^3O_2$, and water.[29,30] Gas products passed through a cold trap (kept at −70 °C) to remove water vapor. Only $^1O_2$, $^3O_2$, and He remained in the downstream gas. The concentration of $^1O_2$ was determined by measuring $^1O_2$ emission ($a^1\Delta_g \rightarrow X^3\sum_g^-$, $v = 0-0$)[31] at 1270 nm in an optical emission cell. Emission from the cell was collected by a plano-



DOI: 10.1021/acs.jpcb.6b11464
J. Phys. Chem. B 2017, 121, 956−966

convex BK7 lens, passed through an optical chopper (SRS model SR540) and a 5 nm bandwidth interference filter centered at 1270 nm (Andover, blocked to 1550 nm). The chopped emission was focused by another plano-convex BK7 lens into a thermoelectrically cooled InGaAs photodetector (Newport 71887 detector and 77055 cooler) coupled with a lock-in amplifier (SRS model SR830). Amplifier output was converted to absolute $^1O_2$ concentration based on a previous calibration.[32] To reduce the residence time, and therefore, the wall- and self-quenching of $^1O_2$, the entire $^1O_2$ generator was continuously pumped down to a pressure of 12.8 Torr using a mechanical pump regulated by a pressure relay. At this pressure, a maximum concentration of $^1O_2$ was available for carrying out ion−molecule reactions.

The $^1O_2$ generator also produced $^3O_2$. However, $^3O_2$ does not react with singlet closed-shell molecules because the reaction is spin-forbidden. The nonreactivity of 8-oxoG ions toward $^3O_2$ has been verified in control experiments that were performed under the same conditions except that $Cl_2$ used in the $^1O_2$ generator was replaced by oxygen gas at the same flow rate.

**2.2. Ion−Molecule Scattering.** The reactions of 8-oxoG ions with $^1O_2$ were carried out on a homemade guided-ion-beam tandem mass spectrometer, which was described in detail previously,[33] along with the operation, calibration and data analysis procedures. The apparatus consists of an ion-source, a radio frequency (rf) hexapole ion guide, a quadrupole mass filter, an rf octopole ion guide surrounded by a scattering cell, a second quadrupole mass filter, and a pulse-counting electron multiplier detector. Both quadrupoles use Extrel 9.5 mm diameter trifilter rods operating at 2.1 MHz to cover a mass/charge ($m/z$) range of 1−500.

A sample solution for generating $[8\text{-oxoG} + H]^+$ was prepared in methanol/water (3:1 vol. ratio) containing 0.05 mM 8-oxoG (≥90%, Enzo) and 1 mM HCl, and that for $[8\text{-oxoG} - H]^-$ was prepared in methanol/water (3:1) containing 0.05 mM 8-oxoG and 0.5 mM NaOH. The solution was sprayed into the ambient atmosphere through an electrospray needle at a flow rate of 0.06 mL/h. The ESI needle was held at 2.2 and −2.2 kV relative to ground for producing positively and negatively charged species, respectively. Charged droplets entered the source chamber of the mass spectrometer through a pressure-reducing desolvation capillary, which was heated to 150 °C and biased at 90 to 150 V for positive ions and −90 to −120 V for negative ones. The distance between the tip of the ESI needle and the sampling orifice of the capillary was 5−10 mm. Liquid aerosols underwent desolvation as they passed through the heated capillary, and were converted to gas-phase ions in the source chamber. Under mild heating conditions, not all of the solvent evaporated, resulting in hydrated ions. It was found that the pure water solution of $[8\text{-oxoG} + H]^+$ resulted in a maximum ion intensity for monohydrated $[8\text{-oxoG} + H]^+\cdot W$ ($W = H_2O$), whereas the solution of $[8\text{-oxoG} - H]^-$ in ethanol/methanol/water (1:2:1) yielded a maximum intensity for $[8\text{-oxoG} - H]^-\cdot W$.

A skimmer with an orifice of 0.99 mm is located 3 mm from the capillary end, separating the source chamber and the hexapole ion guide. The skimmer was biased at 20 V relative to ground for positive ions and −20 V for negative ones. Ions that emerged from the skimmer were transported into the hexapole at a pressure of 24 mTorr, undergoing collisional focusing and cooled to ∼310 K. Ions subsequently passed into a conventional quadrupole for selection of specific reactant ions. Mass-selected reactant ions were collected and focused into the octopole ion guide, which trapped ions in the radial direction, minimizing the loss of the reactant and product ions resulting from scattering. The octopole operated at 2.6 MHz with a peak-to-peak rf amplitude of 600 V. The octopole is surrounded by the scattering cell containing neutral reactant gas. The cell pressure was controlled by a leak valve and measured by a Baratron capacitance manometer (MKS 690 head and 670 signal conditioner). After passing through the scattering cell, remaining reactant ions and product ions drifted to the end of the octopole, and then were mass analyzed by the second quadrupole, and counted by the electron multiplier.

The initial kinetic energy distributions of the reactant ions were determined by a retarding potential analysis (RPA)[34] that measures the intensity of the ion beam while scanning the DC bias voltage applied to the octopole. The DC bias voltage also allowed control of the kinetic energy of reactant ions in the laboratory frame ($E_{Lab}$). $E_{Lab}$ can be converted into the collision energy ($E_{col}$) between reactant ions and $^1O_2$ molecules in the center-of-mass frame using $E_{col} = E_{Lab} \times m_{neutral}/(m_{ion} + m_{neutral})$, where $m_{neutral}$ and $m_{ion}$ are the masses of neutral and ionic reactants, respectively. Intensities of the reactant ion beam were $6 \times 10^4$ counts/s for $[8\text{-oxoG} + H]^+$, $2 \times 10^5$ counts/s for $[8\text{-oxoG} - H]^-$, and $2 \times 10^4$ counts/s for their monohydrates. Initial kinetic energy was 0.75 eV for $[8\text{-oxoG} + H]^+\cdot W_{0,1}$ and 0.96 eV for $[8\text{-oxoG} - H]^-\cdot W_{0,1}$, with an energy spread of 0.6−0.75 eV that corresponds to an $E_{col}$ resolution of ≤0.1 eV.

Reaction cross sections were calculated from the ratios of reactant and product ion intensities at each $E_{col}$ (under single ion−molecule collision conditions), the pressure of $^1O_2$ in the scattering cell (= the gas pressure in the cell × the abundance of $^1O_2$), and the effective cell length. The scattering cell pressure was set at 0.25 mTorr containing 5% of $^1O_2/^3O_2$ and 95% of He. Under these conditions, 8-oxoG ions underwent at most a single collision with $O_2$. Ions also collided with He, but heavy ion-light neutral combination made these collisions insignificant at low $E_{col}$.

The emission intensity of $^1O_2$ was monitored continuously, and its variation (controlled to be within 20%) was corrected for in calculating reaction cross sections. Experiment was repeated multiple times and each time we cycled through different $E_{col}$. Reported data represent an average of four complete data sets. Based on the reproducibility of measurements, the relative error of reaction cross sections (e.g., uncertainty in comparing data at different $E_{col}$) was estimated to be ∼20%.

**2.3. DFT and RRKM Calculations.** Geometries of reactants, intermediates, transition states (TSs), and products were optimized using Gaussian 09,[35] at the B3LYP level of theory paired with the 6-311++G(d,p) basis set. Tautomer/rotamer search was conducted for all reactants, and the most stable conformations were used as the starting structures in reaction PESs and kinetic modeling.

Note that an extended set of density functional theories has been assessed for guanine oxidation intermediates.[36] One concern about using B3LYP in describing guanine oxidation is that the stability of the 8-peroxide of guanine was overestimated by this functional. However, we found that B3LYP was able to predict correct energetics of the endoperoxide vs the 8-peroxide of protonated and deprotonated guanine, because the reactions did not involve significant charge transfer between the $O_2$ moiety and the reactant ions.[9] This hybrid GGA functional has been generally successful in describing the $^1O_2$ oxidation of


DOI: 10.1021/acs.jpcb.6b11464
J. Phys. Chem. B 2017, 121, 956−966

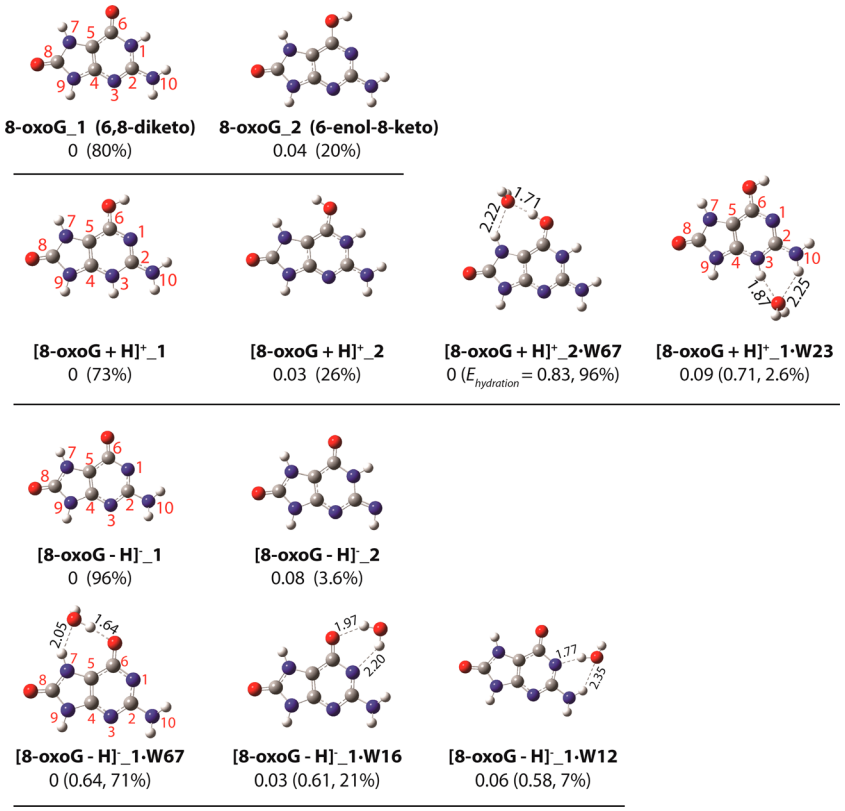


**Figure 1.** Low-lying tautomers/conformers of 8-oxoG, $[8\text{-oxoG} + H]^+\cdot W_{0,1}$, $[8\text{-oxoG} - H]^-\cdot W_{0,1}$. Atomic numbering scheme and nomenclature are presented. Relative energies (eV, with respect to global minima), hydration energies (in parentheses), and thermal populations (in parentheses) were evaluated at B3LYP/6-311++G(d,p) with 298 K thermal corrections.

guanine,[9,37] 9-methylguanine,[10] 6-thioguanine,[38] and histidine.[39,40] We had also benchmarked the PESs for deprotonated 9-methylguanine + $^1O_2$[10] constructed at the B3LYP, M06-2X, ωB97XD, and MP2 levels against the one obtained from multireferential CASSCF(10,8), and found that B3LYP most closely reproduced the CASSCF PES.[10] Restricted-to-unrestricted instabilities were checked. For those without stable wavefunctions in restricted calculations, an unrestricted method was used, and spin contamination was not an issue. All TSs were verified as first-order saddle points, and the vibrational mode associated with an imaginary frequency corresponds to the anticipated reaction pathway. Aside from the local criterion, intrinsic reaction coordinate (IRC) calculations were carried out to identify reactant/product minima connected through the identified TSs.

B3LYP/6-311++G(d,p) calculated vibrational frequencies and zero-point energies (ZPEs) were scaled by a factor of 0.952 and 0.988,[41] respectively. To refine the quality of reaction PESs, the electronic energies of all critical structures along reaction coordinates were recalculated at the B3LYP/aug-cc-pVQZ level using B3LYP/6-311++G(d,p) optimized structures. Potentials (with respect to reactants) in PESs were determined based on the sum of the electronic energies calculated at B3LYP/aug-cc-pVQZ and the 298 K thermal corrections calculated at B3LYP/6-311++G(d,p) (including ZPE). In conformation search for $[8\text{-oxoG} + H]^+$, the MP2/6-311++G(d,p) method was used in addition to B3LYP, aimed at validating the B3LYP−predicted conformers.

The energy gaps between the singlet and the triplet electronic states of $[8\text{-oxoG} + H]^+ + {}^1O_2$ and $[8\text{-oxoG} - H]^- + {}^1O_2$ are 1.65 and 2.10 eV, respectively. Thus, the need for a multireference treatment is alleviated for these systems, as what was found for the $^1O_2$ reaction with neutral, protonated, and deprotonated guanine.[9,10,42] To further ascertain that B3LYP calculations were not invalidated by multireference effects, T1 diagnostic[43] was performed for critical structures, and results suggest that B3LYP is appropriate for the present systems.

RRKM unimolecular rates were calculated with the program of Zhu and Hase,[44] using direct state count algorithm and scaled B3LYP/6-311++G(d,p) frequencies and B3LYP/aug-cc-pVQZ energetics. The orbital angular momentum $L$ for the reaction was estimated from collision cross section ($\sigma_{col}$), i.e., $L = \mu\cdot v_{rel}\cdot(\sigma_{col}/\pi)^{1/2}$, where $\mu$ and $v_{rel}$ are the reduced mass and the relative velocity of collision partners, respectively. Product branching was determined by the ratio of RRKM rates for different channels.

## 3. RESULTS AND DISCUSSION

**3.1. Structures of $[8\text{-oxoG} + H]^+\cdot W_{0,1}$ and $[8\text{-oxoG} - H]^-\cdot W_{0,1}$.** Tautomers/rotamers of neutral, protonated, and deprotonated 8-oxoG as well as their monohydrates were calculated at the B3LYP/6-311++G(d,p) level of theory. All stable structures are presented in Figures S1−S5, and their Cartesian coordinates are provided in the Supporting Information, too. Each conformer has a number suffix to denote the order of stability within its structure category. For hydrates, we included hydration sites in their notations. Representative low-energy conformers for each of the neutral, protonated, and deprotonated series, along with their relative energies and populations, are summarized in Figure 1. The



DOI: 10.1021/acs.jpcb.6b11464
J. Phys. Chem. B 2017, 121, 956−966

populations of various tautomers and rotamers were estimated based on their computed relative stabilities at 298 K.

A total of 16 stable tautomers/rotamers were found for neutral 8-oxoG, arising from keto−enol and amino−imino tautomerization, H migration between N1 and N3 and between N7 and N9, and rotation of side groups. They are gathered in Figure S1, of which the two most significant tautomers, 6,8-diketo and 6-enol-8-keto, are depicted in the top row of Figure 1. Based on B3LYP/6-311++G(d,p) calculations, the 6,8-diketo and 6-enol-8-keto tautomers represent 80 and 20% of the 8-oxoG population at 298 K, respectively. Both DFT (including those in the literature[25,45−49] and in the present work) and MP2[45,46,50] calculations have predicted 6,8-diketo and 6-enol-8-keto as the two lowest-energy gas-phase tautomers of 8-oxoG. But most of the MP2 calculations reported a reversed order of stability between the two tautomers (i.e., the 6-enol-8-keto tautomer was predicted as the global minimum at MP2),[45,46,50] except the most recent MP2/cc-pVDZ work[51] that predicted the same order of stability as DFT. Since the remaining conformations of 8-oxoG have negligible populations, the 6,8-diketo and 6-enol-8-keto tautomers were used as neutral reactants in constructing the protonated and deprotonated structures of 8-oxoG.

Fifteen conformers were identified for protonated $[8\text{-oxoG} + H]^+$ (Figure S2) by protonating different O and N sites in the 6,8-diketo and 6-enol-8-keto tautomers of 8-oxoG. The first two lowest-energy conformers of $[8\text{-oxoG} + H]^+$ lie within 0.1 eV with a calculated thermal population of 73 and 26%, respectively. The most stable protonated conformer is formed by protonation of N3 in the 6-enol-8-keto tautomer of 8-oxoG, and the next by protonation of O6 in the 6,8-diketo tautomer of 8-oxoG. Note that the literature has reported some conformations for $[8\text{-oxoG} + H]^+$ at both B3LYP[47,48] and MP2[49] levels. But the results are incomplete and inconsistent. To avoid systematic errors that might arise from B3LYP calculations, all of the protonated conformations presented in Figure S2 were reoptimized at MP2/6-311++G(d,p). In our study, both B3LYP and MP2 theories predicted the same global minimum structure and the similar order of stabilities, except for $[8\text{-oxoG} + H]^+\_13$ that is unstable at MP2.

We found nine conformers for deprotonated $[8\text{-oxoG} - H]^-$ (Figure S3) via deprotonation of the N1−H, N7−H, N9−H, and the amino group in the 6,8-diketo tautomer of 8-oxoG, and of the N7−H, N9−H, and the enol in the 6-enol-8-keto tautomer of 8-oxoG. Of these, deprotonation of N1−H in 6,8-diketo (or the enol in 6-enol-8-keto) leads to an almost exclusively dominant structure $[8\text{-oxoG} - H]^-\_1$, with a calculated population of 96% at 298 K.

Starting geometries of monohydrated ions were obtained by adding a water molecule to all possible hydration sites in the two lowest-energy protonated conformers (i.e., $[8\text{-oxoG} + H]^+$ _1 and 2) and the lowest-energy deprotonated conformer (i.e., $[8\text{-oxoG} - H]^-\_1$). These structures were then optimized at B3LYP/6-311++G(d,p). All of the converged structures are gathered in Figures S4 and S5, with the water binding sites appended to structure notations. Hydration energy was calculated using $E_{hydraion} = E(\text{bare ion}) + E(H_2O) - E(\text{cluster})$, where $E$(bare ion), $E(H_2O)$, and $E$(cluster) are the B3LYP−calculated energies of bare ion, water and the monohydrate of the same ion conformation, respectively. The lowest-energy protonated monohydrate, $[8\text{-oxoG} + H]^+\_2{\cdot}W67$, has the water binding to its C6-enol and N7−H with $E_{hydration}$ = 0.83 eV, and accounts for a 96% population of the protonated monohydrate at 298 K. The most favorable deprotonated monohydrate is formed also by a water hydrogen-bonded to C6−O and N7−H in $[8\text{-oxoG} - H]^-\_1$ concurrently and denoted as $[8\text{-oxoG} - H]^-\_1{\cdot}W67$ with $E_{hydration}$ = 0.64 eV and a calculated thermal population of 71%. Such cyclic water-binding motifs are similar to those found in hydrated neutral, protonated and deprotonated guanine[9,52,53] and 9-methylguanine.[10]

In sum, our conformation search not only reproduced the neutral,[45−48,50,51] protonated,[48] and deprotonated[47−49,51] 8-oxoG conformers reported in the literature, but identified many new structures. On the basis of their populations calculated at 298 K, $[8\text{-oxoG} + H]^+\_1$, $[8\text{-oxoG} + H]^+\_2{\cdot}W67$, $[8\text{-oxoG} - H]^-\_1$, $[8\text{-oxoG} - H]^-\_1{\cdot}W67$ represent dominant reactants in gas-phase reactions, and were used as starting structures in construction of reaction PESs.

**3.2. Reaction Products and Cross Sections.** We first examined the reactions of $^1O_2$ with bare $[8\text{-oxoG} + H]^+$ and $[8\text{-oxoG} - H]^-$ over the center-of-mass $E_{col}$ range of 0.1−1.0 eV. However, no products were detected, except collision-induced elimination of $H_2O$ and CO from $[8\text{-oxoG} + H]^+$, and elimination of $H_2O$ and $CN_2H_2$ from $[8\text{-oxoG} - H]^-$ at high energies. We had thought it might be because peroxides formed in the reactions are extremely unstable and decayed back to starting reactants during the time-of-flight in the mass spectrometer. This scenario was found in the $^1O_2$ reactions with isolated histidine,[39] guanine,[9] and 9-methylguanine ions,[10] all of which were found to be completely nonreactive because of the fast decomposition of transient adducts. To measure transient species in the latter three systems, we devised reaction routes by using hydrated reactant ions as the target for collisions with $^1O_2$. The point was to stabilize nascent peroxides based on water evaporation cooling arising from gas-phase hydrates. This strategy was proved to be useful in capturing transient endoperoxides of histidine, guanine, and 9-methylguanine.

Following the same idea, we have examined the collisions of $^1O_2$ with $[8\text{-oxoG} + H]^+{\cdot}W$ and $[8\text{-oxoG} - H]^-{\cdot}W$. In contrast to our expectation, no oxidation product was detected for $[8\text{-oxoG} + H]^+{\cdot}W$, either. On the other hand, this approach did work out for the deprotonated system, as product ions were detected at $m/z$ 198 for $[8\text{-oxoG} - H]^-{\cdot}W + {}^1O_2$. Figure 2a shows a representative product ion mass spectrum measured at $E_{col}$ = 0.1 eV. This product can be attributed to liberation of a water ligand from an $O_2$ adduct of $[8\text{-oxoG} - H]^-{\cdot}W$. Reaction cross section ($\sigma_{reaction}$) for $[8\text{-oxoG} - H]^-{\cdot}W + {}^1O_2$ is shown in Figure 2b over the $E_{col}$ range of 0.1 to 0.5 eV, along with the reaction efficiency (estimated from $\sigma_{reaction}/\sigma_{col}$ in which $\sigma_{col}$ is the greater of the ion-induced dipole capture cross section[54] and hard-sphere collision cross section). $\sigma_{reaction}$ increases with decreasing $E_{col}$, indicating that there is no activation barrier above reactants. As for any exothermic reactions, the reaction efficiency is significant only at low energies. Increasing the amount of energy available decreased the probability of the reaction; as a consequence, the efficiency decreases rapidly at high $E_{col}$, eventually becoming zero at the energy above 0.3 eV.

A similar $E_{col}$ dependence of $\sigma_{reaction}$ was observed for $[G - H]^-{\cdot}W + {}^1O_2$[9] and $[9MG - H]^-{\cdot}W + {}^1O_2$.[10] However, the reaction efficiency (measured at the lowest $E_{col}$) for $[8\text{-oxoG} - H]^-{\cdot}W$ increases by a factor of 1.6 compared to that for $[G - H]^-{\cdot}W$, and by a factor of 2.2 compared to that for $[9MG - H]^-{\cdot}W$.



DOI: 10.1021/acs.jpcb.6b11464
J. Phys. Chem. B 2017, 121, 956−966

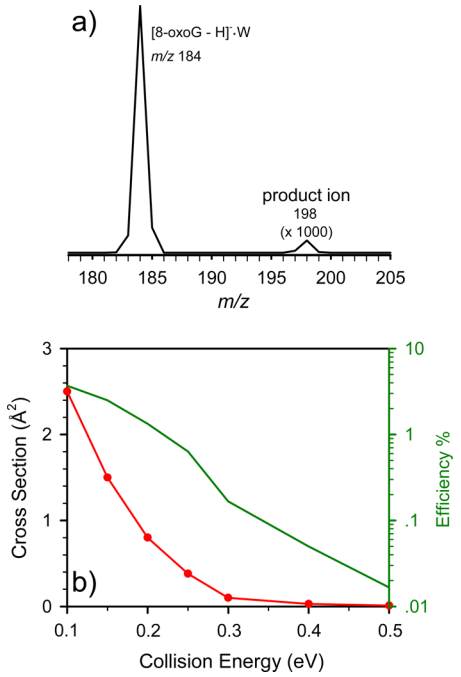


**Figure 2.** (a) Product mass spectrum for $[8\text{-oxoG} - H]^-\cdot W + {}^1O_2$ obtained at $E_{col}$ = 0.1 eV, and (b) reaction cross section and efficiency (dark green line against the right axis) for $[8\text{-oxoG} - H]^-\cdot W + {}^1O_2$.

**3.3. Nonreactivity of $[8\text{-oxoG} + H]^+\cdot W_{0,1}$.** *Three Concerted $^1O_2$ Addition Pathways for Dehydrated [8-oxoG + H]$^+$.* To address the origin of the nonreactivity of $[8\text{-oxoG} + H]^+$ with $^1O_2$, we turn to computational evidence. A PES constructed at B3LYP/aug-cc-pVQZ//B3LYP/6-311++G(d,p) is presented in Figure 3a, with reactants shown near the center at zero potential energy. Guided by the mechanisms in Scheme 1, we first looked at the possibility of 4,5-cycloaddition of $^1O_2$ to $[8\text{-oxoG} + H]^+$. This corresponds to reactants → TS1$^+$ → [4,5-dioxetane + H]$^+$ in Figure 3a. [4,5-Dioxetane + H]$^+$, if formed, would evolve to hydroperoxides, including $[4\text{-OOH}^7\text{-}8\text{-oxoG} + H]^+$ (via intramolecular H transfer at TS2$^+$; the superscription in notation indicates the position from which H is abstracted), $[5\text{-OOH}^9\text{-}8\text{-oxoG} + H]^+$ via TS3$^+$, $[5\text{-OOH}^3\text{-}8\text{-oxoG} + H]^+$ via TS4$^+$, and $[4\text{-OOH}^6\text{-}8\text{-oxoG} + H]^+$ via TS5$^+$.

To further examine the initial 4,5-addition, a 56 × 56 grid of potential surface for governing the addition was generated at the B3LYP/6-311++G(d,p) level using a relaxed PES scan, and is visualized in Figure 3b. r(C4−O) and r(C5−O), which characterize the distance between the C4−C5 bond and the $O_2$ moiety, are considered as reaction coordinates and each decreases from 2.8/3.0 to 1.4 Å at an interval of 0.025 Å. All the other bond lengths and bond angles were optimized at each point of the PES. On this PES, there is a deep well corresponding to [4,5-dioxetane + H]$^+$ that is separated from reactants by a saddle point located at TS1$^+$. A minimum energy pathway along the intrinsic reaction coordinate is projected onto the PES. A movie depicting this IRC trajectory is available in the Supporting Information. The reaction features synchronous addition of $O_2$ across the C4−C5 bond but with an asymmetrical TS geometry with r(C4−O) = 1.6 Å and r(C5−O) = 2.3 Å.

A close examination of Figure 3b reveals another potential well that corresponds to a 2,5-endoperoxide of $[8\text{-oxoG} + H]^+$. To the best of our knowledge, 2,5-addition was never considered for 8-oxoG + $^1O_2$. This led us to explore a 2D-PES and IRC trajectory along r(C2−O) and r(C5−O). The results in Figure 3c demonstrate that 2,5-cycloaddition follows a concerted pathway and has nearly equal r(C2−O) = 1.95 Å and r(C5−O) = 1.9 Å at TS6$^+$. This pathway is depicted in the movie available in the Supporting Information. Inspired by the discovery of 2,5-addition, we explored the possibility of 2,4-addition by running another PES scan along r(C2−O) and r(C4−O). As shown in Figure 3d, the scan results in a third concerted cycloaddition path, leading to formation of $[2,4\text{-OO-}8\text{-oxoG} + H]^+$ with an activation barrier at TS7$^+$ (see the accompanying movie in the Supporting Information). The two new addition pathways are presented in the left portion of the PES in Figure 3a. For the sake of comparison, we replotted the IRC trajectory for 2,5-addition in Figure 3d, by following the changes of r(C2−O) and r(C4−O) during addition. Comparison of the 2,5- and 2,4-addition trajectories in Figure 3d indicates that the trajectory may switch between the two pathways during propagation toward products.

What was unexpected from the PES calculations is that the activation barriers for 2,5-addition (TS6$^+$, 0.25 eV) and 2,4-addition (TS7$^+$, 0.34 eV) are much lower than that for the conventional 4,5-addition (TS1$^+$, 1.03 eV). However, all pathways are kinetically blocked by barriers above reactants and therefore discounted at low $E_{col}$.

*Changes of $^1O_2$ Addition to [8-oxoG + H]$^+$ in the Presence of a Water Ligand.* One complication in the interpretation of the $[8\text{-oxoG} + H]^+$ reaction is the change of the favorable reactant conformation upon hydration. Of the first two most stable conformers, $[8\text{-oxoG} + H]^+\_2$ differs from $[8\text{-oxoG} + H]^+\_1$ in the orientation of the 6-enol group and N1H−N3H tautomerization. Whereas $[8\text{-oxoG} + H]^+\_2$ accounts for only 26% of the dehydrated reactant ions, it becomes the dominant structure (96%) for the monohydrate. As an interesting note, $[8\text{-oxoG} + H]^+\_1$ would again predominate over $[8\text{-oxoG} + H]^+\_2$ in aqueous solution, on the basis of the energies computed using the polarized continuum model[55] at the B3LYP/6-311++G(d,p) level.

Despite of the structural differences, $[8\text{-oxoG} + H]^+\_2\cdot W67$, referred to as $[8\text{-oxoG} + H]^+\cdot W$ henceforth, follows nearly the same reaction pathways as those for $[8\text{-oxoG} + H]^+\_1$. As illustrated in Figure 4, $[8\text{-oxoG} + H]^+\cdot W$ may undergo 4,5-addition of $O_2$ at TS1$^+\cdot$W (0.71 eV above reactants) and gives rise to hydrated dioxetane $[4,5\text{-OO-}8\text{-oxoG} + H]^+\cdot W$. Alternatively, $O_2$ may add to C2−C5 of $[8\text{-oxoG} + H]^+\cdot W$ at TS6$^+\cdot$W (0.32 eV), producing $[2,5\text{-OO-}8\text{-oxoG} + H]^+\cdot W$. Movies depicting $[8\text{-oxoG} + H]^+\cdot W$ to $[4,5\text{-OO-}8\text{-oxoG} + H]^+\cdot W$ and to $[2,5\text{-OO-}8\text{-oxoG} + H]^+\cdot W$ are available in the Supporting Information. Compared to dehydrated $[8\text{-oxoG} + H]^+\_1$, the activation barrier for 4,5-addition to $[8\text{-oxoG} + H]^+\cdot W$ decreases by 0.32 eV whereas that for 2,5-addition increases by 0.07 eV. We had explored the possibility of forming $[2,4\text{-OO-}8\text{-oxoG} + H]^+\cdot W$; however, starting geometries with a 2,4-endo structure either converged to $[2,5\text{-OO-}8\text{-oxoG} + H]^+\cdot W$ or decayed back to reactants. Again, due to the associated high and tight activation barriers, neither of $[4,5\text{-OO-}8\text{-oxoG} + H]^+\cdot W$ and $[2,5\text{-OO-}8\text{-oxoG} + H]^+\cdot W$ formed at low $E_{col}$.

**3.4. $^1O_2$ Addition to $[8\text{-oxoG} - H]^-$ Becomes Stepwise, Rendering Reaction Exothermic.** *Short-Lived Products in the Absence of Water.* The most intriguing result from the reaction PES in Figure 5a is that $[8\text{-oxoG} - H]^-$ does not undergo cycloaddition with $^1O_2$, which contrasts with the commonly proposed mechanism in Scheme 1. The ion−



DOI: 10.1021/acs.jpcb.6b11464
J. Phys. Chem. B 2017, 121, 956−966

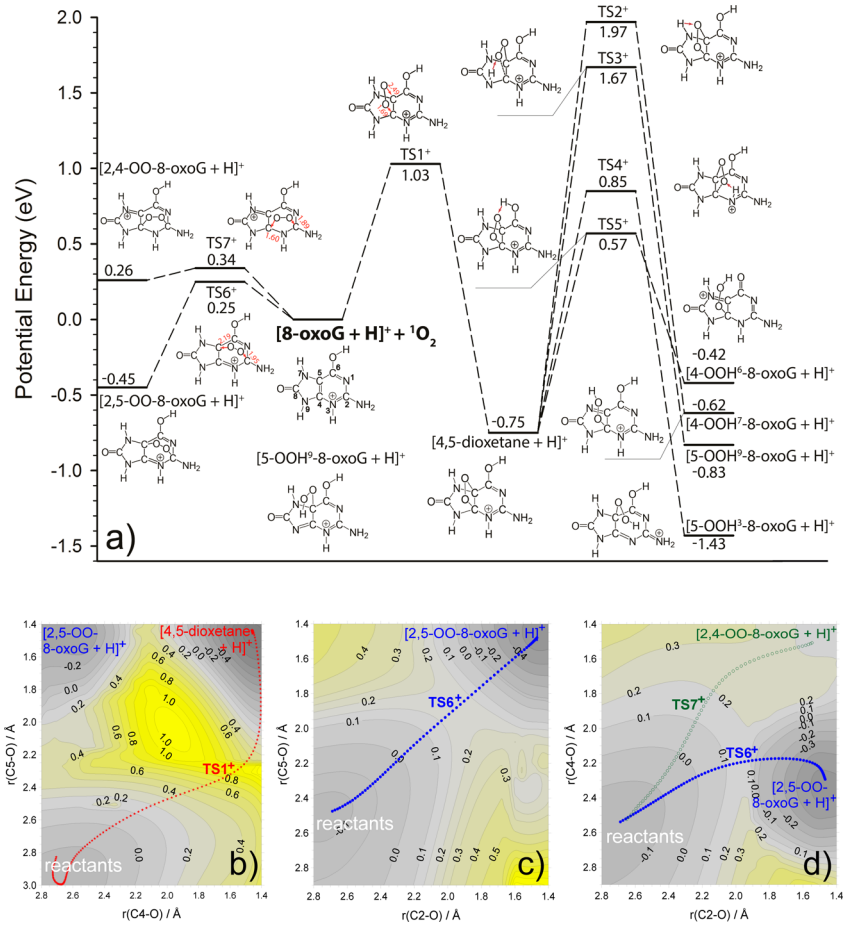


**Figure 3.** (a) Reaction coordinate for $[8\text{-oxoG} + H]^+ + {}^1O_2$. Energies (relative to reactants) were calculated at B3LYP/aug-cc-pVQZ//B3LYP/6-311++G(d,p), including thermal corrections at 298 K. For TSs, vibrational modes corresponding to imaginary frequencies are indicated by displacement vectors; (b–d) 2D-PESs for the addition of $^1O_2$ to the C4–C5, C2–C5, and C2–C4 positions of $[8\text{-oxoG} + H]^+$, respectively. Numbers in the contour maps are potential energies calculated at B3LYP/6-311++G(d,p). Colored lines represent IRC trajectories. Movies (in MPEG format) depicting IRC trajectories in b, c, and d are available in the Supporting Information.

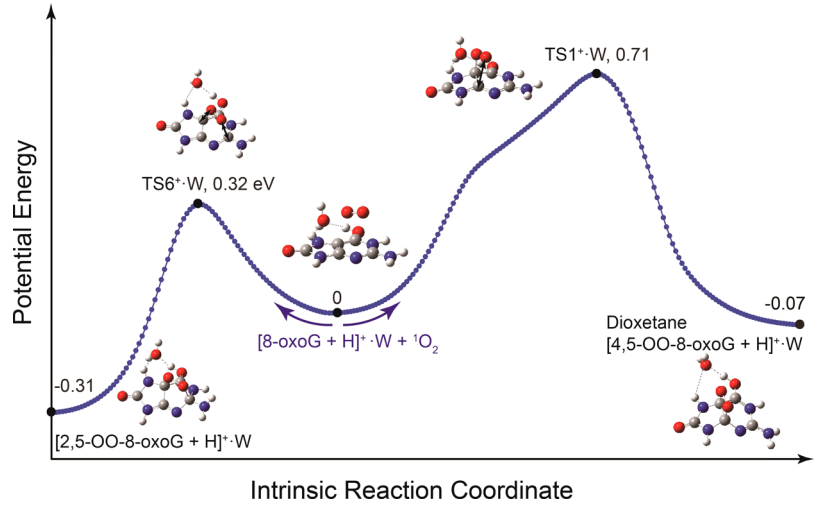


**Figure 4.** Reaction PES for $[8\text{-oxoG} + H]^+\cdot W + {}^1O_2$, constructed at B3LYP/6-311++G(d,p). Energies of critical structures were refined at B3LYP/aug-cc-pVQZ. Movies (in MPEG format) for (right) $[8\text{-oxoG} + H]^+\cdot W \rightarrow TS1^+\cdot W \rightarrow [4,5\text{-OO-8-oxoG} + H]^+\cdot W$ and (left) $[8\text{-oxoG} + H]^+\cdot W \rightarrow TS6^+\cdot W \rightarrow [2,5\text{-OO-8-oxoG} + H]^+\cdot W$ are available in the Supporting Information.

molecule collision leads to formation of a precursor complex between the collision partners, with an electrostatic binding energy of 0.77 eV with respect to reactants. The precursor is rather floppy, with large amplitude of intermolecular motion. It allows repeated encounters between reactants, increasing the probability of the $^1O_2$ attack at the C5-terminal. This results in a low-barrier pathway that leads to formation of a terminal peroxide $[5\text{-OO-8-oxoG} - H]^-$. This mechanism resembles a



DOI: 10.1021/acs.jpcb.6b11464
J. Phys. Chem. B 2017, 121, 956–966

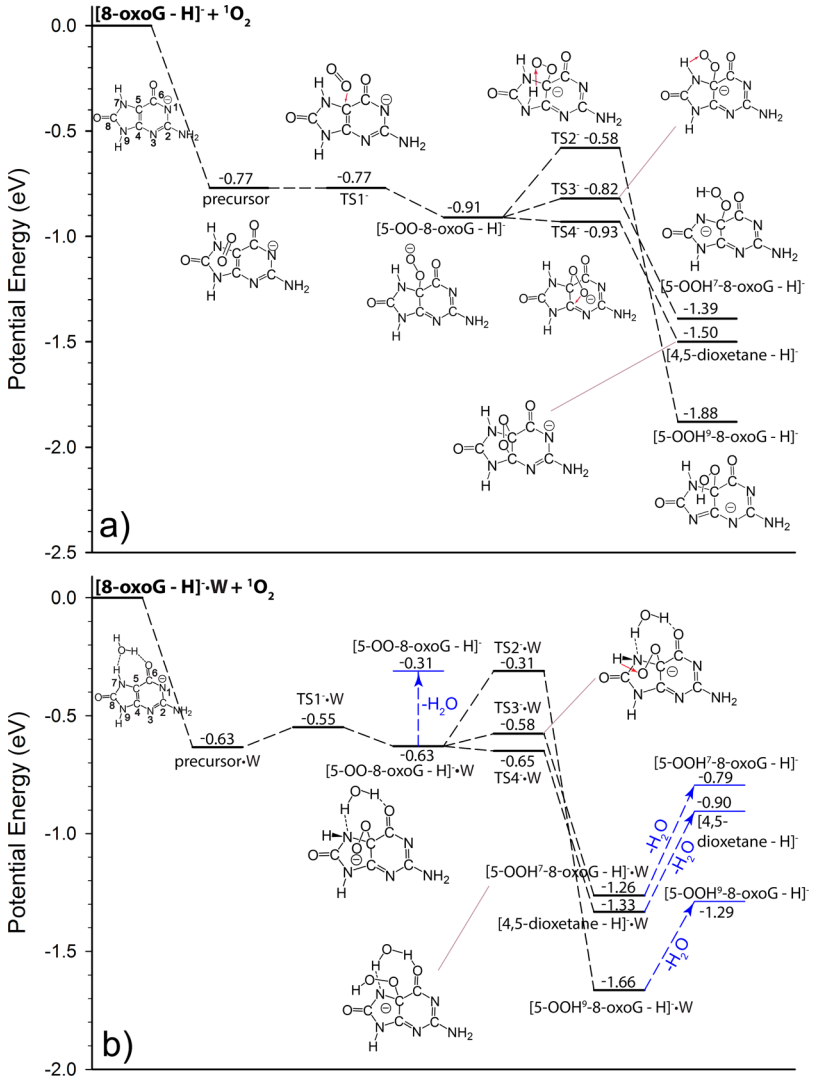


**Figure 5.** Reaction coordinates for (a) $[8\text{-oxoG} - H]^- + {}^1O_2$, and (b) $[8\text{-oxoG} - H]^-\cdot W + {}^1O_2$. Energies (relative to reactants) were calculated at B3LYP/aug-cc-pVQZ//B3LYP/6-311++G(d,p), including thermal corrections at 298 K. For TSs, vibrational modes corresponding to imaginary frequencies are indicated by displacement vectors. A movie (in MPEG format) of $[8\text{-oxoG} - H]^-$ along the favorable reaction pathway is available in the Supporting Information.

DFT−predicted $^1O_2$ addition reaction toward neutral 8-oxoG.[37] The terminal addition becomes possible because $^1O_2$ has some nucleophilic character due to a high lying HOMO,[40] although $^1O_2$ is generally shown to be electrophilic. The activation barrier TS1$^-$ for the C5-terminal addition is equal to the precursor in energy. Based on NBO charge analysis, the negative charge remains on the $[8\text{-oxoG} - H]^-$ moiety in most of the reaction TSs and intermediates.

$[5\text{-OO-8-oxoG} - H]^-$ serves as a common intermediate from which different end products stem. $[5\text{-OO-8-oxoG} - H]^-$ may undergo intramolecular H transfer to $[5\text{-OOH}^9\text{-8-oxoG} - H]^-$ via TS2$^-$, or $[5\text{-OOH}^7\text{-8-oxoG} - H]^-$ via TS3$^-$. But the dominant process should be formation of 4,5-dioxetane via ring-closure at TS4$^-$. In $[5\text{-OO-8-oxoG} - H]^-$, r(C5−O) reaches 1.42 Å, while the other O is located 2.79 Å away from C4. Moving on to TS4$^-$, the two bond lengths are shortened to 1.38 and 2.53 Å, respectively, indicative of an asymmetric transition state. Finally, r(C5−O) and r(C4−O) reach equilibrium distances of 1.45 and 1.49 Å, respectively, in $[4,5\text{-dioxetane} - H]^-$. The electronic energy of TS4$^-$ is slightly higher than that of $[5\text{-OO-8-oxoG} - H]^-$ by 0.01 eV. But inclusion of thermal corrections in the PES shifts the energy of TS4$^-$ below $[5\text{-OO-8-oxoG} - H]^-$ by 0.02 eV. Furthermore, TS4$^-$ is relatively "loose" in that its imaginary frequency is only 61 cm$^{-1}$. It indicates that $[5\text{-OO-8-oxoG} - H]^-$, once formed, could continue downhill "barrierlessly" to 4,5-dioxetane. An energetically favorable reaction pathway thus corresponds to "$[8\text{-oxoG} - H]^- + {}^1O_2 \rightarrow$ precursor $\rightarrow$ TS1$^-$ $\rightarrow$ $[5\text{-OO-8-oxoG} - H]^- \rightarrow$ TS4$^-$ $\rightarrow$ $[4,5\text{-dioxetane} - H]^-$". A movie of the molecule along this favorable pathway is available in the Supporting Information. No other addition pathways were located, although such possibility could not be ruled out.

The aforementioned favorable pathway has no participating activation barriers that are situated above reactants, therefore $[5\text{-OO-8-oxoG} - H]^-$ and/or $[4,5\text{-dioxetane} - H]^-$ were expected to form at low $E_{col}$. However, none of these products was present in product mass spectra. Note that the mechanistic importance of an intermediate/product also depends on its lifetime, so we used the RRKM theory to model the unimolecular kinetics of these intermediates (including the precursor complex). No barrier is expected for decay of the precursor to reactants in excess of dissociation asymptote, thus


DOI: 10.1021/acs.jpcb.6b11464
J. Phys. Chem. B 2017, 121, 956−966

an orbiting transition state[56] was assumed. The rotational quantum number $K$ was treated as active in evaluating rate constant $k(E, J)$, and all $(2J + 1)K$ levels were counted as shown by eq 1:

$$k(E, J) = \frac{d}{h}\frac{\sum_{K=-J}^{J} G[E - E_0 - E_r^{\dagger}(J, K)]}{\sum_{K=-J}^{J} N[E - E_r(J, K)]} \quad (1)$$

where $d$ is the reaction path degeneracy, $G$ is the sum of accessible states from 0 to $E - E_0 - E_r^{\dagger}$ in the TS, $N$ is the energized reactant's density of states, $E$ is the system energy, $E_0$ is the activation energy, and $E_r$ and $E_r^{\dagger}$ are the rotational energies for the reactant and the TS, respectively. Properties of complexes and TSs were described by B3LYP−calculated frequencies, polarizabilities, and moments of inertia.

RRKM results have provided critical kinetic insight. At the $E_{col}$ regime below 0.2 eV (where a complex-mediated mechanism is important), the precursor, [5-OO-8-oxoG − H]$^-$, [5-OOH$^7$-8-oxoG − H]$^-$, and [4,5-dioxetane − H]$^-$ interconverted quickly, except [5-OOH$^9$-8-oxoG − H]$^-$ that formed slowly and was thus insignificant. Interconversion time is 2−3 ps between the precursor and [5-OO-8-oxoG − H]$^-$, 2−3 ns between [5-OO-8-oxoG − H]$^-$ and [5-OOH$^7$-8-oxoG − H]$^-$ is, and <1 ns between [5-OO-8-oxoG − H]$^-$ and [4,5-dioxetane − H]$^-$. Therefore, these complexes could be lumped together, of which [4,5-dioxetane − H]$^-$ constituted more than 70% of the ensemble. The total lifetime of these complexes accounted for the duration that the system was trapped within adducts. This time length was in turn determined by how fast the precursor complex decayed back to reactants. The rate constant for "precursor → reactants" is $5 \times 10^7$ s$^{-1}$ at $E_{col}$ = 0.1 eV, and increases to $3.5 \times 10^8$ s$^{-1}$ at 0.2 eV. This corresponds to a total complex lifetime of 3−20 ns that was way too short compared to the time-of-flight of product ions ($\sim 10^2$ $\mu$s) through the octopole ion guide and the second quadrupole of the mass spectrometer. As a result, all products decomposed into reactants before reaching the ion detector.

Note that the electron detachment energy for [8-oxoG − H]$^-$ was calculated to be 2.93 eV, which is beyond the maximum $E_{col}$. Therefore, electron detachment could be disregarded in collisions. Charge transfer of [8-oxoG − H]$^-$ + $^1O_2$ → [8-oxoG − H] + $O_2^-$ is endothermic by 1.50 eV, and thus is unlikely to be relevant in the experiment, either.

*Distribution of Stable Products in the Presence of Water.* Among the conformers of deprotonated monohydrates, [8-oxoG − H]$^-$_1·W67 has a B3LYP−calculated population of 71% at 298 K and was used as the starting structure in the reaction PES for [8-oxoG − H]$^-$·W + $^1O_2$. Due to the identical lowest-energy ion conformation in the isolated and monohydrated [8-oxoG − H]$^-$, the PESs for [8-oxoG − H]$^-$·W + $^1O_2$ (Figure 5b) and [8-oxoG − H]$^-$ + $^1O_2$ (Figure 5a) share common features. A precursor complex and four peroxides may form between [8-oxoG − H]$^-$·W and $^1O_2$. We have located TSs connecting complexes to each other and to products. Except the water ligand, the structures of the complexes, and TSs shown in Figure 5b are identical to those in Figure 5a. To differentiate the similar species between the isolated and monohydrated systems, we have included a water ligand in the acronyms for hydrated structures.

At the initial stage, [8-oxoG − H]$^-$·W follows the same route as [8-oxoG − H]$^-$, forming [5-OO-8-oxoG − H]$^-$·W. But the fate of [5-OO-8-oxoG − H]$^-$ changed after hydration. It may decay back to the precursor via TS1$^-$·W, or eliminate water via an orbiting TS, or interconvert to hydroperoxides and dioxetane via TS2$^-$·W, TS3$^-$·W, and TS4$^-$·W, respectively. On the basis of the RRKM analysis, the product branching ratios from [5-OO-8-oxoG − H]$^-$·W are 2.8 (decay to the precursor): 35.5 (water elimination): 0 (formation of [5-OOH$^9$-8-oxoG − H]$^-$·W): 10.7 ([5-OOH$^7$-8-oxoG − H]$^-$·W): 51 ([4,5-dioxetane − H]$^-$·W) at $E_{col}$ = 0.1 eV, changing to 3.1:35.2:0:11.7:50 at 0.2 eV. Assuming that [5-OOH$^7$-8-oxoG − H]$^-$·W and [4,5-dioxetane − H]$^-$·W liberated the water ligand during the time-of-flight, the dominating products of $m/z$ = 198 in mass spectra should be [4,5-dioxetane − H]$^-$, followed by [5-OO-8-oxoG − H]$^-$ and [5-OOH$^7$-8-oxoG − H]$^-$ as summarized below:

$$[8\text{-oxoG} - H]^-\cdot W + {}^1O_2 \rightarrow [4,5\text{-dioxetane} - H]^- + H_2O \qquad \Delta H_{rxn} = -0.90 \text{ eV} \quad (2)$$

$$\rightarrow [5\text{-OOH}^7\text{-8-oxoG} - H]^- + H_2O \qquad \Delta H_{rxn} = -0.79 \text{ eV} \quad (3)$$

$$\rightarrow [5\text{-OO-8-oxoG} - H]^- + H_2O \qquad \Delta H_{rxn} = -0.31 \text{ eV} \quad (4)$$

The contrast between the complete kinetic blockage of [8-oxoG − H]$^-$ + $^1O_2$ and the exothermic products of [8-oxoG − H]$^-$·W + $^1O_2$ once again demonstrates the kinetic influence of microsolvation. That is the energized peroxides disposed of sufficient internal excitation via water elimination and accompanying product kinetic energy release, so that peroxides did not decompose themselves. For the reactions of eqs 2−4, water dissociation energy is between 0.32 and 0.47 eV. This energy was compensated by the oxidation reaction enthalpy. Thus, there is no penalty of becoming endothermic for the overall reactions.

An interesting observation is that the reaction of [8-oxoG − H]$^-$·W + $^1O_2$ is extremely inefficient. The maximum efficiency is <4%, despite the reaction being exothermic and without barriers above reactants. Two factors may contribute to the low reaction efficiency. First, the water ligand of [8-oxoG − H]$^-$·W may physically quench $^1O_2$. Second, there may exist excitation transfer-induced dissociation,[57] i.e., [8-oxoG − H]$^-$·W + $^1O_2$ → [8-oxoG − H]$^-$ + $H_2O$ + $^3O_2$. Unfortunately, neither of these two processes could be measured or computed directly.

## 4. CONCLUSION

8-oxoG is one of the most common DNA lesions resulting from reactive oxygen species and ionizing radiation, and it becomes more oxidizable than guanine. We have investigated the $^1O_2$ oxidation of 8-oxoG in protonated, deprotonated, and hydrated states on the basis of ion-scattering mass spectrometric measurements augmented with molecular potential and kinetic simulations, from which the dependence of reaction on initial conditions are examined. To eliminate radicals accompanying photosensitized oxidation,[58] in this work $^1O_2$ was generated by the reaction of $H_2O_2$ with $Cl_2$ in basic solution. The $^1O_2$ oxidation of [8-oxoG + H]$^+$ is initiated by formation of endoperoxides via concerted addition of $O_2$ to the C4−C5, C2−C5, or C2−C4 positions of [8-oxoG + H]$^+$, akin to what was proposed for neutral 8-oxoG (Scheme 1). But all reaction pathways are hampered by high activation barriers that render [8-oxoG + H]$^+$ nonreactive with $^1O_2$. However, this is not the case for the deprotonated system. The initial oxidation stage for [8-oxoG − H]$^-$ switches to a terminal addition of $^1O_2$


DOI: 10.1021/acs.jpcb.6b11464
J. Phys. Chem. B 2017, 121, 956−966

to the C5 position only. Reaction continues from the ensuing $[5\text{-OO-8-oxoG} - H]^-$, evolving to 4,5-dioxetane and 5-hydroperoxide that are analogous to the oxidation products of 8-oxoG in solution. The dichotomy between protonated and deprotonated reactant systems implies pH dependence of the initial oxidation of 8-oxoG. Biological significance of such pH dependence is obvious considering the fact that $pK_a$(N1) of 8-oxoG is 8.5[47] and therefore 8-oxoG exists as a mixture of neutral and deprotonated (>7%) forms in the physiological pH range.

Reactions are affected by microsolvation. For $[8\text{-oxoG} + H]^+$, the presence of a water ligand leads to a different global minimum and modifies reaction pathways. For $[8\text{-oxoG} - H]^-$, hydration stabilizes peroxide products, so that they could be captured by mass spectrometer.

To the best of our knowledge, there was no experimental assessment of the activation barriers associated with the initial $^1O_2$ oxidation of 8-oxoG. The $E_{col}$ dependence of the reaction cross section for $[8\text{-oxoG} - H]^-\cdot W + {}^1O_2$ measured in this work has for the first time confirmed that the $^1O_2$ addition to deprotonated 8-oxoG has no activation barriers above reactants, and reaction is sufficiently exothermic that it is possible to eliminate the water ligand from scattering complexes. This data serves as a critical benchmark for related computation.

## ■ ASSOCIATED CONTENT

### Supporting Information

The Supporting Information is available free of charge on the ACS Publications website at DOI: 10.1021/acs.jpcb.6b11464.

Structures and Cartesian coordinates for tautomer/rotamers of 8-oxoG, $[8\text{-oxoG} + H]^+\cdot W_{0,1}$, $[8\text{-oxoG} - H]^-\cdot W_{0,1}$ (PDF)

MPEG movies for reaction trajectories in Figures 3b–d, 4, and 5a (ZIP)

## ■ AUTHOR INFORMATION


### Corresponding Author

*E-mail: jianbo.liu@qc.cuny.edu; Telephone: 1-718-997-3271.

### ORCID

Jianbo Liu: 0000-0001-9577-3740


### Notes

The authors declare no competing financial interest.

## ■ ACKNOWLEDGMENTS

This work was supported by the National Science Foundation (Grant No. CHE 1464171).

## ■ REFERENCES


(1) Sheu, C.; Foote, C. S. Endoperoxide Formation in a Guanosine Derivative. *J. Am. Chem. Soc.* **1993**, *115*, 10446–10447.

(2) Niles, J. C.; Wishnok, J. S.; Tannenbaum, S. R. Spiroiminodihydantoin Is the Major Product of the 8-Oxo-7,8-Dihydroguanosine Reaction with Peroxynitrite in the Presence of Thiols and Guanosine Photooxidation by Methylene Blue. *Org. Lett.* **2001**, *3*, 963–966.

(3) Ye, Y.; Muller, J. G.; Luo, W.; Mayne, C. L.; Shallop, A. J.; Jones, R. A.; Burrows, C. J. Formation of $^{13}C$-, $^{15}N$-, and $^{18}O$-Labeled Guanidinohydantoin from Guanosine Oxidation with Singlet Oxygen. Implications for Structure and Mechanism. *J. Am. Chem. Soc.* **2003**, *125*, 13926–13927.

(4) Ravanat, J.-L.; Martinez, G. R.; Medeiros, M. H. G.; Di Mascio, P.; Cadet, J. Mechanistic Aspects of the Oxidation of DNA Constituents Mediated by Singlet Molecular Oxygen. *Arch. Biochem. Biophys.* **2004**, *423*, 23–30.

(5) Cadet, J.; Ravanat, J.-L.; Martinez, G. R.; Medeiros, M. H. G.; Di Mascio, P. Singlet Oxygen Oxidation of Isolated and Cellular DNA: Product Formation and Mechanistic Insights. *Photochem. Photobiol.* **2006**, *82*, 1219–1225.

(6) Gimisis, T.; Cismas, C. Isolation, Characterization, and Independent Synthesis of Guanine Oxidation Products. *Eur. J. Org. Chem.* **2006**, *2006*, 1351–1378.

(7) Neeley, W. L.; Essigmann, J. M. Mechanisms of Formation, Genotoxicity, and Mutation of Guanine Oxidation Products. *Chem. Res. Toxicol.* **2006**, *19*, 491–505.

(8) Cadet, J.; Douki, T.; Ravanat, J.-L. Oxidatively Generated Damage to the Guanine Moiety of DNA: Mechanistic Aspects and Formation in Cells. *Acc. Chem. Res.* **2008**, *41*, 1075–1083.

(9) Lu, W.; Liu, J. Capturing Transient Endoperoxide in the Singlet Oxygen Oxidation of Guanine. *Chem. - Eur. J.* **2016**, *22*, 3127–3138.

(10) Lu, W.; Teng, H.; Liu, J. How Protonation and Deprotonation of 9-Methylguanine Alter Its Singlet $O_2$ Addition Path: About the Initial Stage of Guanine Nucleoside Oxidation. *Phys. Chem. Chem. Phys.* **2016**, *18*, 15223–15234.

(11) Marchetti, B.; Karsili, T. N. V. An Exploration of the Reactivity of Singlet Oxygen with Biomolecular Constituents. *Chem. Commun. (Cambridge, U. K.)* **2016**, *52*, 10996–10999.

(12) Bruner, S. D.; Norman, D. P. G.; Verdine, G. L. Structural Basis for Recognition and Repair of the Endogenous Mutagen 8-Oxoguanine in DNA. *Nature* **2000**, *403*, 859–866.

(13) Lovell, M. A.; Markesbery, W. R. Ratio of 8-Hydroxyguanine in Intact DNA to Free 8-Hydroxyguanine Is Increased in Alzheimer Disease Ventricular Cerebrospinal Fluid. *Arch. Neurol.* **2001**, *58*, 392–396.

(14) Zhang, J.; Perry, G.; Smith, M. A.; Robertson, D.; Olson, S. J.; Graham, D. G.; Montine, T. J. Parkinson's Disease Is Associated with Oxidative Damage to Cytoplasmic DNA and RNA in Substantia Nigra Neurons. *Am. J. Pathol.* **1999**, *154*, 1423–1429.

(15) Xu, X.; Muller, J. G.; Ye, Y.; Burrows, C. J. DNA-Protein Cross-Links between Guanine and Lysine Depend on the Mechanism of Oxidation for Formation of C5 vs C8 Guanosine Adducts. *J. Am. Chem. Soc.* **2008**, *130*, 703–709.

(16) *Oxidative Stress*; Sies, H., Ed.; Academic Press, 1985; p 507.

(17) Boiteux, S.; Radicella, J. P. Base Excision Repair of 8-Hydroxyguanine Protects DNA from Endogenous Oxidative Stress. *Biochimie* **1999**, *81*, 59–67.

(18) Sheu, C.; Foote, C. S. Photosensitized Oxygenation of a 7,8-Dihydro-8-Oxoguanosine Derivative. Formation of Dioxetane and Hydroperoxide Intermediates. *J. Am. Chem. Soc.* **1995**, *117*, 474–477.

(19) Buchko, G. W.; Wagner, J. R.; Cadet, J.; Raoul, S.; Weinfeld, M. Methylene Blue-Mediated Photooxidation of 7,8-Dihydro-8-Oxo-2′-Deoxyguanosine. *Biochim. Biophys. Acta, Gene Struct. Expression* **1995**, *1263*, 17–24.

(20) Hickerson, R. P.; Prat, F.; Muller, J. G.; Foote, C. S.; Burrows, C. J. Sequence and Stacking Dependence of 8-Oxoguanine Oxidation: Comparison of One-Electron vs Singlet Oxygen Mechanisms. *J. Am. Chem. Soc.* **1999**, *121*, 9423–9428.

(21) Duarte, V.; Gasparutto, D.; Yamaguchi, L. F.; Ravanat, J.-L.; Martinez, G. R.; Medeiros, M. H. G.; Di Mascio, P.; Cadet, J. Oxaluric Acid as the Major Product of Singlet Oxygen-Mediated Oxidation of 8-Oxo-7,8-Dihydroguanine in DNA. *J. Am. Chem. Soc.* **2000**, *122*, 12622–12628.

(22) Martinez, G. R.; Medeiros, M. H. G.; Ravanat, J.-L.; Cadet, J.; Di Mascio, P. $[^{18}O]$-Labeled Singlet Oxygen as a Tool for Mechanistic Studies of 8-Oxo-7,8-Dihydroguanine Oxidative Damage: Detection of Spiroiminodihydantoin, Imidazolone and Oxazolone Derivatives. *Biol. Chem.* **2002**, *383*, 607–617.

(23) McCallum, J. E. B.; Kuniyoshi, C. Y.; Foote, C. S. Characterization of 5-Hydroxy-8-Oxo-7,8-Dihydroguanosine in the Photosensitized Oxidation of 8-Oxo-7,8-Dihydroguanosine and Its Rearrangement to Spiroiminodihydantoin. *J. Am. Chem. Soc.* **2004**, *126*, 16777–16782.

(24) Martinez, G. R.; Ravanat, J.-L.; Cadet, J.; Gennari de Medeiros, M. H.; Di Mascio, P. Spiroiminodihydantoin Nucleoside Formation




DOI: 10.1021/acs.jpcb.6b11464
J. Phys. Chem. B 2017, 121, 956–966

from 2′-Deoxyguanosine Oxidation by [$^{18}$O-Labeled] Singlet Molecular Oxygen in Aqueous Solution. *J. Mass Spectrom.* **2007**, *42*, 1326−1332.
(25) Munk, B. H.; Burrows, C. J.; Schlegel, H. B. An Exploration of Mechanisms for the Transformation of 8-Oxoguanine to Guanidinohydantoin and Spiroiminodihydantoin by Density Functional Theory. *J. Am. Chem. Soc.* **2008**, *130*, 5245−5256.
(26) Henderson, P. T.; Delaney, J. C.; Muller, J. G.; Neeley, W. L.; Tannenbaum, S. R.; Burrows, C. J.; Essigmann, J. M. The Hydantoin Lesions Formed from Oxidation of 7,8-Dihydro-8-Oxoguanine Are Potent Sources of Replication Errors in Vivo. *Biochemistry* **2003**, *42*, 9257−9262.
(27) Raoul, S.; Cadet, J. Photosensitized Reaction of 8-Oxo-7,8-Dihydro-2′-Deoxyguanosine: Identification of 1-(2-Deoxy-*β*-D-Erythro-Pentofuranosyl)Cyanuric Acid as the Major Singlet Oxygen Oxidation Product. *J. Am. Chem. Soc.* **1996**, *118*, 1892−1898.
(28) Marcus, R. A. Unimolecular Dissociations and Free-Radical Recombination Reactions. *J. Chem. Phys.* **1952**, *20*, 359−364.
(29) Midey, A.; Dotan, I.; Viggiano, A. A. Temperature Dependences for the Reactions of $O^-$ and $O_2^-$ with $O_2(a^1\Delta_g)$ from 200 to 700 K. *J. Phys. Chem. A* **2008**, *112*, 3040−3045.
(30) Fang, Y.; Liu, F.; Bennett, A.; Ara, S.; Liu, J. Experimental and Trajectory Study on Reaction of Protonated Methionine with Electronically Excited Singlet Molecular Oxygen ($a^1\Delta_g$): Reaction Dynamics and Collision Energy Effects. *J. Phys. Chem. B* **2011**, *115*, 2671−2682.
(31) Lafferty, W. J.; Solodov, A. M.; Lugez, C. L.; Fraser, G. T. Rotational Line Strengths and Self-Pressure-Broadening Coefficients for the 1.27 Mm, $a^1\Delta_g$-$X^3\Sigma_g^-$, V = 0−0 Band of $O_2$. *Appl. Opt.* **1998**, *37*, 2264−2270.
(32) Liu, F.; Fang, Y.; Chen, Y.; Liu, J. Reactions of Deprotonated Tyrosine and Tryptophan with Electronically Excited Singlet Moleuclar Oxygen ($a^1\Delta_g$): A Guided-Ion-Beam Scattering, Statistical Modeling, and Trajectroy Study. *J. Phys. Chem. B* **2012**, *116*, 6369−6379.
(33) Fang, Y.; Liu, J. Reaction of Protonated Tyrosine with Electronically Excited Singlet Molecular Oxygen ($a^1\Delta_g$): An Experimental and Trajectory Study. *J. Phys. Chem. A* **2009**, *113*, 11250−11261.
(34) Ervin, K. M.; Armentrout, P. B. Translational Energy Dependence of $Ar^+ + XY \rightarrow ArX^+ + Y$ (XY = $H_2$, $D_2$, Hd) from Thermal to 30 eV C.M. *J. Chem. Phys.* **1985**, *83*, 166−189.
(35) Frisch, M. J.; Trucks, G. W.; Schlegel, H. B.; Scuseria, G. E.; Robb, M. A.; Cheeseman, J. R.; Scalmani, G.; Barone, V.; Mennucci, B.; Petersson, G. A.; Nakatsuji, H.; Caricato, M.; Li, X.; Hratchian, H. P.; Izmaylov, A. F.; Bloino, J.; Zheng, G.; Sonnenberg, J. L.; Hada, M.; Ehara, M.; Toyota, K.; Fukuda, R.; Hasegawa, J.; Ishida, M.; Nakajima, T.; Honda, Y.; Kitao, O.; Nakai, H.; Vreven, T.; J. A. Montgomery, J.; Peralta, J. E.; Ogliaro, F.; Bearpark, M.; Heyd, J. J.; Brothers, E.; Kudin, K. N.; Staroverov, V. N.; Keith, T.; Kobayashi, R.; Normand, J.; Raghavachari, K.; Rendell, A.; Burant, J. C.; Iyengar, S. S.; Tomasi, J.; Cossi, M.; Rega, N.; Millam, J. M.; Klene, M.; Knox, J. E.; Cross, J. B.; Bakken, V.; Adamo, C.; Jaramillo, J.; Gomperts, R.; Stratmann, R. E.; Yazyev, O.; Austin, A. J.; Cammi, R.; Pomelli, C.; Ochterski, J. W.; Martin, R. L.; Morokuma, K.; Zakrzewski, V. G.; Voth, G. A.; Salvador, P.; Dannenberg, J. J.; Dapprich, S.; Daniels, A. D.; Farkas, O.; Foresman, J. B.; Ortiz, J. V.; Cioslowski, J.; Fox, D. J. *Gaussian 09*; Revision D.01; Gaussian, Inc: Wallingford, CT, 2013.
(36) Grüber, R.; Monari, A.; Dumont, E. Stability of the Guanine Endoperoxide Intermediate: A Computational Challenge for Density Functional Theory. *J. Phys. Chem. A* **2014**, *118*, 11612−11619.
(37) Dumont, E.; Gruber, R.; Bignon, E.; Morell, C.; Moreau, Y.; Monari, A.; Ravanat, J.-L. Probing the Reactivity of Singlet Oxygen with Purines. *Nucleic Acids Res.* **2016**, *44*, 56−62.
(38) Zou, X.; Zhao, H.; Yu, Y.; Su, H. Formation of Guanine-6-Sulfonate from 6-Thioguanine and Singlet Oxygen: A Combined Theoretical and Experimental Study. *J. Am. Chem. Soc.* **2013**, *135*, 4509−4515.
(39) Liu, F.; Lu, W.; Fang, Y.; Liu, J. Evolution of Oxidation Dynamics of Histidine: Non-Reactivity in the Gas Phase, Peroxides in Hydrated Clusters and pH Dependecne in Solution. *Phys. Chem. Chem. Phys.* **2014**, *16*, 22179−22191.
(40) Méndez-Hurtado, J.; López, R.; Suárez, D.; Menéndez, M. I. Theoretical Study of the Oxidation of Histidine by Singlet Oxygen. *Chem. - Eur. J.* **2012**, *18*, 8437−8447.
(41) Alecu, I. M.; Zheng, J.; Zhao, Y.; Truhlar, D. G. Computational Thermochemistry: Scale Factor Databases and Scale Factors for Vibrational Requencies Obtained from Electronic Model Chemistries. *J. Chem. Theory Comput.* **2010**, *6*, 2872−2887.
(42) Dumont, E.; Grueber, R.; Bignon, E.; Morell, C.; Aranda, J.; Ravanat, J.-L.; Tunon, I. Singlet Oxygen Attack on Guanine: Reactivity and Structural Signature within the B-DNA Helix. *Chem. - Eur. J.* **2016**, *22*, 12358−12362.
(43) Lee, T. J.; Taylor, P. R. A Diagnostic for Determining the Quality of Single-Reference Electron Correlation Methods. *Int. J. Quantum Chem.* **1989**, *36*, 199−207.
(44) Zhu, L.; Hase, W. L. *A General RRKM Program(QCPE 644), Quantum Chemistry Program Exchange*; Chemistry Department, University of Indiana: Bloomington, 1993.
(45) Cysewski, P. An Ab Initio Study of the Tautomeric and Coding Properties of 8-Oxo-Guanine. *J. Chem. Soc., Faraday Trans.* **1998**, *94*, 3117−3125.
(46) Gu, J.; Leszczynski, J. Influence of the Oxygen at the C8 Position on the Intramolecular Proton Transfer in C8-Oxidative Guanine. *J. Phys. Chem. A* **1999**, *103*, 577−584.
(47) Jang, Y. H.; Goddard, W. A., III; Noyes, K. T.; Sowers, L. C.; Hwang, S.; Chung, D. S. First Principles Calculations of the Tautomers and p$K_a$ Values of 8-Oxoguanine: Implications for Mutagenicity and Repair. *Chem. Res. Toxicol.* **2002**, *15*, 1023−1035.
(48) Verdolino, V.; Cammi, R.; Munk, B. H.; Schlegel, H. B. Calculation of p$K_a$ Values of Nucleobases and the Guanine Oxidation Products Guanidinohydantoin and Spiroiminodihydantoin Using Density Functional Theory and a Polarizable Continuum Model. *J. Phys. Chem. B* **2008**, *112*, 16860−16873.
(49) Uddin, K. M.; Poirier, R. A. Computational Study of the Deamination of 8-Oxoguanine. *J. Phys. Chem. B* **2011**, *115*, 9151−9159.
(50) Venkateswarlu, D.; Leszczynski, J. Tautomeric Equilibria in 8-Oxopurines: Implications for Mutagenicity. *J. Comput.-Aided Mol. Des.* **1998**, *12*, 373−382.
(51) Lu, Z.; Beckstead, A. A.; Kohler, B.; Matsika, S. Excited State Relaxation of Neutral and Basic 8-Oxoguanine. *J. Phys. Chem. B* **2015**, *119*, 8293−8301.
(52) Hanus, M.; Ryjáček, F.; Kabeláč, M.; Kubař, T.; Bogdan, T. V.; Trygubenko, S. A.; Hobza, P. Correlated Ab Initio Study of Nucleic Acid Bases and Their Tautomers in the Gas Phase, in a Microhydrated Environment and in Aqueous Solution. Guanine: Surprising Stabilization of Rare Tautomers in Aqueous Solution. *J. Am. Chem. Soc.* **2003**, *125*, 7678−7688.
(53) Chandra, A. K.; Nguyen, M. T.; Uchimaru, T.; Zeegers-Huyskens, T. Protonation and Deprotonation Enthalpies of Guanine and Adenine and Implications for the Structure and Energy of Their Complexes with Water: Comparison with Uracil,Thymine, and Cytosine. *J. Phys. Chem. A* **1999**, *103*, 8853−8860.
(54) Troe, J. Statistical Adiabatic Channel Model of Ion-Neutral Dipole Capture Rate Constants. *Chem. Phys. Lett.* **1985**, *122*, 425−430.
(55) Tomasi, J.; Mennucci, B.; Cammi, R. Quantum Mechanical Continuum Solvation Models. *Chem. Rev.* **2005**, *105*, 2999−3093.
(56) Rodgers, M. T.; Ervin, K. M.; Armentrout, P. B. Statistical Modeling of Collision-Induced Dissociation Thresholds. *J. Chem. Phys.* **1997**, *106*, 4499−4508.
(57) Viggiano, A. A.; Midey, A.; Eyet, N.; Bierbaum, V. M.; Troe, J. Dissociative Excitation Transfer in the Reaction of $O_2$ ($a^1\Delta_g$) with $OH^-(H_2O)_{1,2}$ Clusters. *J. Chem. Phys.* **2009**, *131*, 094303.
(58) Foote, C. S. Mechanisms of Photosensitized Oxidation. *Science* **1968**, *162*, 963−970.


DOI: 10.1021/acs.jpcb.6b11464
*J. Phys. Chem. B* 2017, 121, 956−966